JOURNAL OF GEOPHYSICAL RESEARCH, VOL. 103, NO. D14, PAGES 16,999–17,007, JULY 27, 1998

Estimates of radiative forcing due to modeled increases in tropospheric ozone

J. M. Haywood[1]

AOS Program, Princeton University, Princeton, New Jersey

M. D. Schwarzkopf and V. Ramaswamy

Geophysical Fluid Dynamics Laboratory (GFDL), Princeton University, Princeton, New Jersey

Abstract. The GFDL R30 general circulation model (GCM) and a fixed dynamical heating model (FDHM) are used to assess the instantaneous and adjusted radiative forcing due to changes in tropospheric ozone caused by anthropogenic activity. Ozone perturbations from the GFDL global chemical transport model are applied to the GCM, and the instantaneous solar and terrestrial radiative forcings are calculated excluding and including clouds. The FDHM is used to calculate the adjusted radiative forcing at the tropopause. The net global annual mean adjusted radiative forcing, including clouds, ranges from +0.29 to +0.35 W m^{-2} with ~80% of this forcing being in the terrestrial spectrum. If stratospheric adjustment is ignored, the forcing increases by ~10%, and if clouds are ignored, the radiative forcing increases by a further 20–30%. These results are in reasonable agreement with earlier studies and suggest that changes in tropospheric ozone due to anthropogenic emissions exert a global mean radiative forcing that is of similar magnitude but of opposite sign to the direct forcing of sulfate aerosols.

1. Introduction

In recent years, the concentrations of certain atmospheric gases and aerosol particles have increased as a direct consequence of anthropogenic activity [e.g., *Intergovernmental Panel on Climate Change* (*IPCC*), 1996]. These species may exert a considerable influence on the climate of the Earth by influencing the radiative balance of the Earth/atmosphere system. A measure of the potential climatic influence of these constituents is the adjusted radiative forcing [*IPCC*, 1990, 1994, 1996] which is defined as the change in the net irradiance at the tropopause due to the inclusion of the anthropogenic species after allowing stratospheric temperatures to adjust to radiative equilibrium while surface and tropospheric temperatures are held fixed. Two-dimensional (2-D) modeling estimates of the radiative forcing due to increases in tropospheric ozone include those of *Hauglustaine et al.* [1994] who estimated the instantaneous radiative forcing to be +0.55 W m^{-2} and *Forster et al.* [1996] who used the output from two different 2-D chemical transport models (CTMs) and found adjusted radiative forcings of +0.30 and +0.51 W m^{-2}. The 3-D modeling estimates include those of *Chalita et al.* [1994] who estimated the instantaneous radiative forcing to be +0.28 W m^{-2}, *Berntsen et al.* [1997] who estimated the adjusted radiative forcing to be +0.26 and +0.28 W m^{-2} depending on the radiative transfer code used, and *Roelofs et al.* [1997] who estimated the adjusted radiative forcing to be +0.42 W m^{-2}. This study uses the climate from a general circulation model (GCM) and a fixed dynamical heating model (FDHM) in conjunction with the new preindustrial and present-day tropospheric ozone climatologies from the global chemical transport model of *Levy et al.* [1997] to assess the solar and terrestrial radiative forcing due to anthropogenically induced changes in tropospheric ozone. Section 2 describes the method used for the calculations, and section 3 briefly investigates the climatologies of *Levy et al.* [1997]. Sections 4 and 5 describe the instantaneous radiative forcing when clouds are excluded and included in the GCM calculations, and section 6 describes the seasonal cycle of the instantaneous radiative forcing. The adjusted radiative forcing estimated from the FDHM is described in section 7, and section 8 provides a discussion and conclusions.

2. Method

The Geophysical Fluid Dynamics Laboratory (GFDL) R30 GCM described by *Wetherald and Soden* [1995] is used to determine the instantaneous radiative forcing due to tropospheric ozone changes in this investigation. The spatial resolution of the GCM is ~420 by 250 km at the equator, and there are 14 levels in the vertical. Cloud is assumed to fill a grid box completely when a certain height dependent relative humidity threshold is reached. The 26-band two-stream δ-Eddington solar radiation code of *Freidenreich and Ramaswamy* [1997] replaces the original radiation code of *Lacis and Hansen* [1974] within the GCM. The terrestrial radiation code is based on that of *Schwarzkopf and Fels* [1991] modified to include most of the relevant trace gases and a new water vapor continuum formulation. Absorption by ozone, carbon dioxide, water vapor, and other gaseous species such as oxygen, nitrous oxide and methane, and Rayleigh scattering by gaseous constituents are accounted for by these two radiation codes. The radiative transfer codes are called twice in the GCM calculations. The first call to the radiation codes uses the climatological ozone distribution from the GCM [*Wetherald and Soden*, 1995] and does not include the ozone perturbation but determines the radia-

[1]Now at Meteorological Research Flight, DERA, Farnborough, Hants, England.

Paper number 98JD01348.
0148-0227/98/98JD-01348$09.00

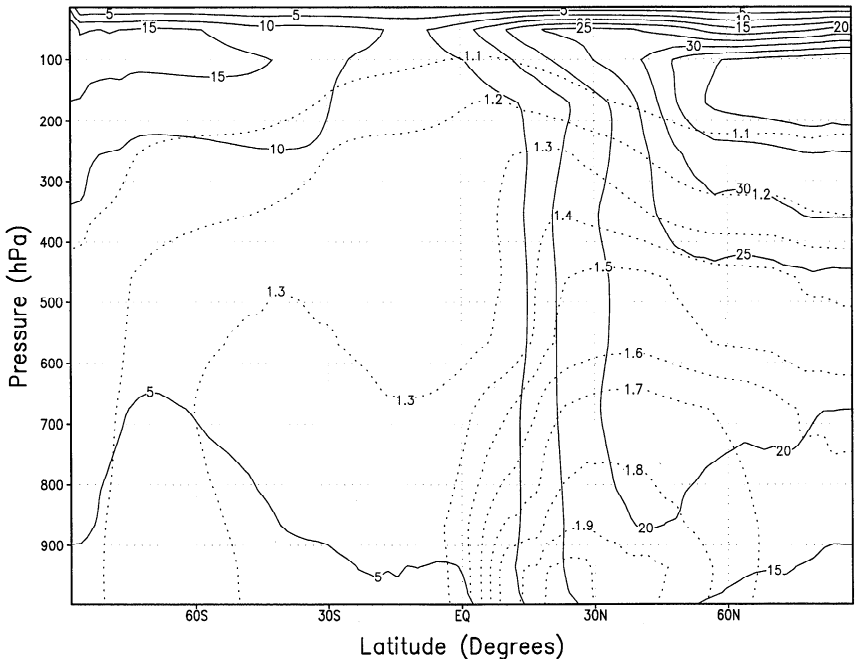

Figure 1. Change in zonal annual-mean ozone concentrations between present and preindustrial conditions from the ozone climatologies of *Levy et al.* [1997]. The solid lines indicate the change in ppbv, and the dotted lines indicate the fractional change in ozone concentrations.

tive heating rates which determine the dynamical evolution of the GCM. The second call to the radiation codes is purely diagnostic and includes the monthly mean ozone perturbation from the global chemical transport model (GCTM) of *Levy et al.* [1997] but does not affect the radiative heating rates in the GCM; the dynamics of the model are therefore unaffected by the ozone perturbation. The instantaneous radiative forcing of ozone is determined as the difference between the net irradiances at the tropopause in the first and second calls to the radiation codes. The tropopause is defined by linear interpolation from a pressure of 100 hPa at the equator to 300 hPa at the poles [*Ramaswamy et al.*, 1992] and is zonally invariant. The monthly mean instantaneous radiative forcing diagnostics are averaged to provide an annual-mean instantaneous radiative forcing diagnostic. The global mean radiative forcing will show a degree of interannual variability due to the daily variability in the GCM fields of, for example, temperature, moisture, surface reflectance, and cloud amount; these sources of variation are not investigated. *Haywood and Ramaswamy* [1998] used a similar procedure in calculating the direct radiative forcing of sulfate and black carbon aerosols.

A FDHM with an identical radiation code and horizontal and vertical resolution to the GCM is also used to investigate the instantaneous and adjusted radiative forcings. Monthly mean instantaneous radiative forcings are calculated by applying the monthly mean insolation, solar zenith angle, temperature, specific humidity, cloud amount, and surface reflectance from the R30 model to the FDHM. Random cloud overlap is assumed in the FDHM. As in the GCM, two calls to the radiative transfer codes are made, one excluding the ozone perturbation, the other including the monthly mean ozone perturbation. The difference in the net solar and terrestrial irradiances at the tropopause between the two calls to the radiation code yields the instantaneous solar and terrestrial radiative forcings, with the tropopause being defined as in the GCM calculations. Thus it is possible to compare the instantaneous radiative forcing calculated by the GCM with that calculated by the FDHM; since the radiative transfer codes of the GCM and the FDHM are identical, any differences in the instantaneous radiative forcing result from the use of monthly mean fields in the FDHM.

The adjusted radiative forcing at the tropopause is calculated in the FDHM using the fixed dynamical heating approximation [e.g., *Fels and Kaplan*, 1975; *Fels et al.*, 1980]. A similar method to that used in calculating the instantaneous radiative forcing is applied. The difference is that when the ozone perturbation is applied, dynamical heating rates are held fixed, and stratospheric temperatures are allowed to adjust to radiative-dynamical equilibrium; tropospheric temperatures and other parameters, including water vapor and clouds, continue to be held at the unperturbed values. Annual-mean values for the adjusted radiative forcing at the tropopause are then calculated by averaging the monthly mean adjusted radiative forcings. Although other methods of calculating the adjusted radiative forcing have been recently proposed [e.g., *Forster et al.*, 1997], this method is pursued as it allows direct comparison between the monthly mean instantaneous and the adjusted radiative forcings.

3. Changes in Ozone Concentrations

Figure 1 shows the annual-average zonal mean changes in ozone concentrations in ppbv from the GCTM of *Levy et al.* [1997] together with the fractional change in ozone concentrations. The ozone perturbations exceed 40 ppbv between 100 and 200 hPa at latitudes of between 60°N and 90°N. In the northern hemisphere, changes of up to 30 ppbv occur in the upper troposphere, changes of ~20–30 ppbv occur in the midtroposphere, and changes of around 15 ppbv occur at the surface. The changes in the troposphere in the southern hemi-

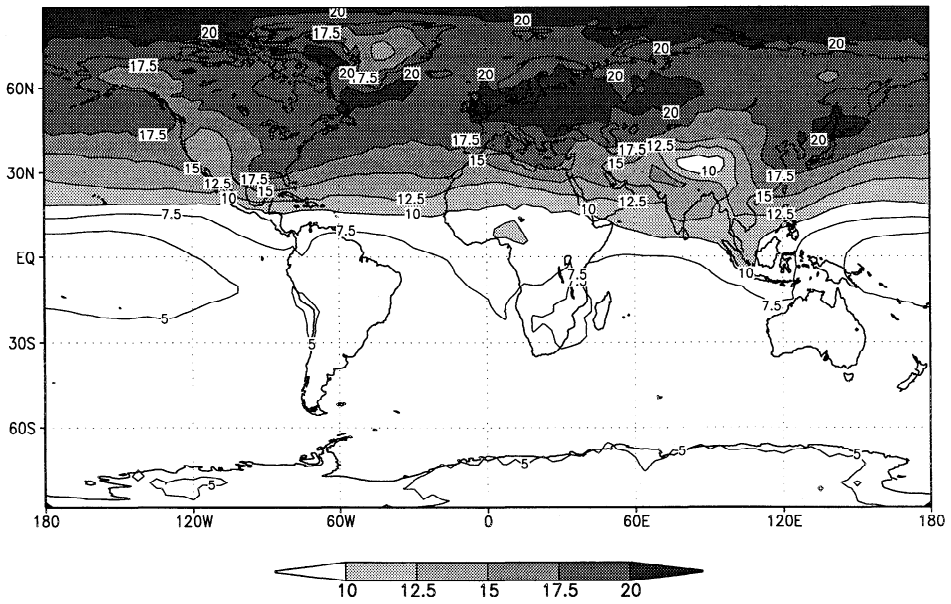

Figure 2. Present minus preindustrial annual-mean ozone concentrations (Dobson units (DU)).

sphere are less significant and are between 3 and 10 ppbv at all altitudes. The fractional changes in ozone range from approximately a factor of 1.1 in the upper troposphere to over a factor of 2.0 close to the surface between 20° and 30°N. It should be noted here that the GCTM model of *Levy et al.* [1997] describes changes in tropospheric ozone due to increased anthropogenic emissions of NO_x; chlorofluorocarbon (CFC) chemistry is not included, thus the observed depletion of ozone in the stratosphere [e.g., *WMO*, 1995] will not be represented. In fact, the ozone perturbations from the GCTM show enhanced ozone concentrations due to anthropogenic emissions of NO_x. The majority of the results presented here include the perturbations in the stratosphere from the *Levy et al.* [1997] model; we shall see in sections 5 and 7 that the radiative effects due to ozone perturbations in the stratosphere are small when compared to those due to the perturbations in the troposphere.

Figure 2 shows the geographic distribution of the annual-average total column changes in ozone in Dobson units (DU) between preindustrial and present-day scenarios. The changes in column ozone are approximately zonally uniform with maximum values of over 20 DU occurring at midlatitudes in the northern hemisphere. The northern and southern hemisphere changes in column ozone are 14.1 and 6.1 DU, respectively. The global mean perturbation is therefore 10.1 DU, of which 2.2 DU come from the stratosphere (see Figure 1). The tropospheric mean column burden is ~7.9 DU which is lower than that determined by *Berntsen et al.* [1997] (9.4 DU) and by one of the CTMs that is used in the 2-D study of *Forster et al.* [1996] (9.4 DU) but higher than that determined by *Roelofs et al.* [1997] (7.3 DU). The spatial and vertical distribution of the perturbations in the troposphere is qualitatively similar for all of the models. It is extremely difficult to assess which of these perturbations is most accurate because there is no historical record of preindustrial ozone concentrations except at a few ground-based locations [*Marenco et al.*, 1994, and references therein].

The ozone perturbations have a substantially different spatial resolution to well-mixed greenhouse gases such as carbon dioxide. Additionally, the spatial distribution of the ozone perturbations differs from the anthropogenic column perturbation due to sulfate, black carbon, organic carbon, and dust aerosols [e.g., *Kasibhatla et al.*, 1997; *Cooke and Wilson*, 1996; *Liousse et al.*, 1996; *Tegen and Fung*, 1995]. Generally, aerosol column perturbations tend to be more closely confined to the areas of emission than the ozone column perturbations which are more zonal in nature.

4. Clear-Sky Instantaneous Radiative Forcing

Figures 3a–3c show the annual-mean solar, terrestrial, and net instantaneous radiative forcing at the tropopause when cloud fields are excluded from the GCM. The global annual-mean shortwave and terrestrial instantaneous radiative forcings are estimated to be +0.02 and +0.44 W m^{-2}, yielding a global annual-mean net instantaneous radiative forcing excluding clouds of +0.46 W m^{-2}.

Figure 3a shows that the annual-mean instantaneous solar radiative forcing is a strong function of the surface reflectance; there is little radiative forcing over the oceans where the surface reflectance is low, and the maximum radiative forcing occurs over the ice sheets of the northern hemisphere where the surface reflectance is highest, and the change in total column ozone is high in these regions (see Figure 2). The high surface reflectance leads to a larger difference in reflected irradiance from the surface when the ozone perturbation is applied resulting in a more positive radiative forcing. Similar results have been found for strongly absorbing tropospheric aerosols [e.g., *Haywood et al.*, 1997; *Haywood and Ramaswamy*, 1997].

Figure 3b shows that the maximum annual-mean instantaneous terrestrial radiative forcing in excess of +0.9 W m^{-2} occurs at latitudes of between ~20°N and 50°N; the maximum terrestrial radiative forcing is displaced to the south of areas of maximum column ozone change (see Figure 2). This is because the terrestrial forcing is most sensitive to ozone perturbations in the upper troposphere [e.g., *Lacis et al.*, 1990]. The difference between the zonal mean surface temperature and the upper tropospheric temperature in the R30 model is larger at

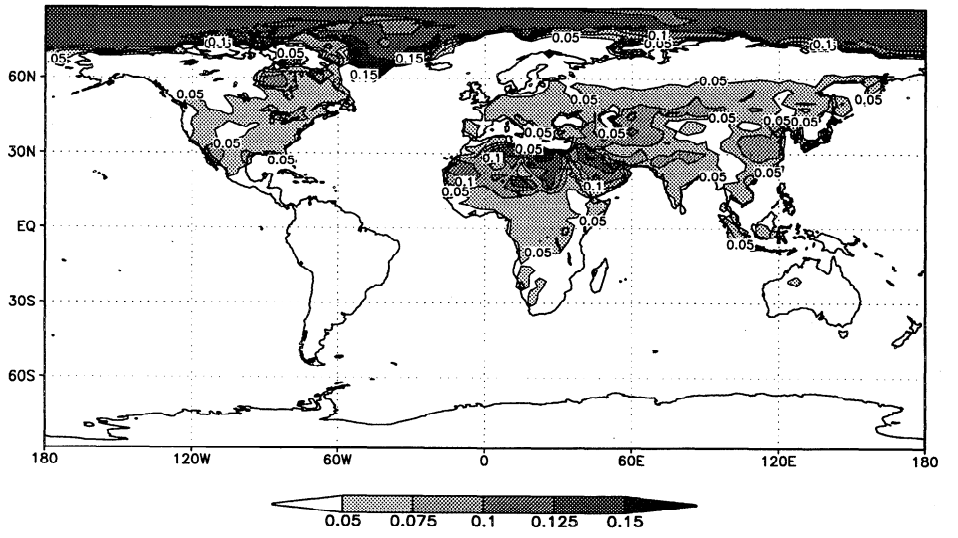

a) NH=+0.04Wm^{-2}, SH=+0.01Wm^{-2}, Global=+0.02Wm^{-2}

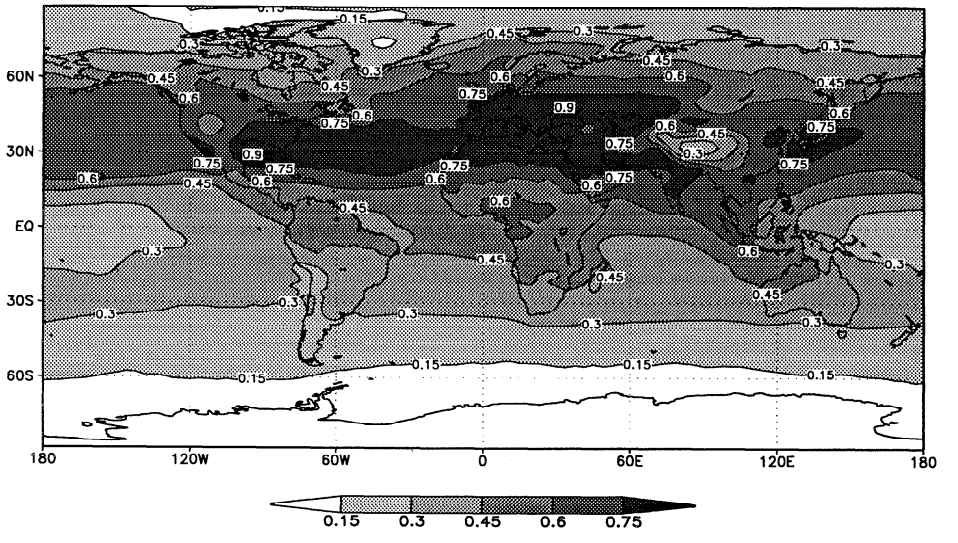

b) NH=+0.58Wm^{-2}, SH=+0.29Wm^{-2}, Global=+0.44Wm^{-2}

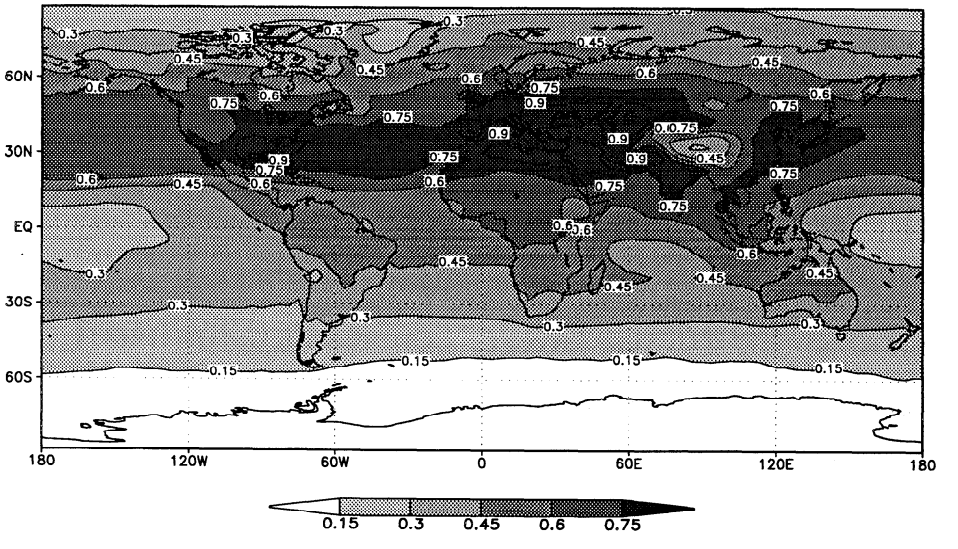

c) NH=+0.62Wm^{-2}, SH=+0.30Wm^{-2}, Global=+0.46Wm^{-2}

Figure 3. (a) Solar, (b) terrestrial, and (c) net instantaneous annual-mean radiative forcing (W m^{-2}) for clear skies calculated using the general circulation model (GCM) as described in the text.

the equator (300–210 K) than at the poles (240–220 K), hence the greater sensitivity at lower latitudes.

Figure 3c shows the combined effect of both solar and terrestrial radiative forcing excluding clouds. The magnitude of the northern hemisphere net instantaneous radiative forcing is approximately double that of the southern hemisphere, the total annual-mean global net radiative forcing being +0.46 W m^{-2}.

5. Total Sky Instantaneous Radiative Forcing

Figures 4a–4c show the annual-mean solar, terrestrial, and net instantaneous radiative forcing, respectively, when the GCM cloud fields are included in the calculations. The global annual-mean shortwave and terrestrial instantaneous radiative forcings at the tropopause are estimated to be +0.07 and +0.31 W m^{-2}, respectively, yielding an annual-mean global net instantaneous radiative forcing of +0.38 W m^{-2}.

As in the clear-sky case, the ratio of the northern hemisphere to the southern hemisphere instantaneous radiative forcing is similar for the net radiative forcings. The instantaneous solar, terrestrial, and net radiative forcings in the northern hemisphere are approximately double that in the southern hemisphere.

Comparison of Figure 4a with Figure 3a shows that the inclusion of the cloud distribution increases the global solar instantaneous radiative forcing by approximately a factor of 3.5. In contrast to the clear-sky case, substantial contributions to the solar instantaneous radiative forcing now exist over cloudy oceanic areas due to the greatly increased underlying reflectance (see section 4).

Comparison of Figure 4b with Figure 3b shows that the inclusion of cloud decreases the global instantaneous terrestrial radiative forcing by a factor of approximately 1.4. This is because when clouds are included, the effective tropospheric emission temperature is lowered, leading to a reduction in the terrestrial energy absorbed by the ozone in the upper troposphere. Thus the areas most affected by the inclusion of clouds occur where deep convective clouds are predicted in the GCM, particularly near the intertropical convergence zone. In those areas where the GCM predicts substantial areas of low cloud, such as in the Atlantic and Pacific Oceans, there is little effect on the net radiative forcing because the effective emission temperature is similar to that for clear skies.

The overall effect of clouds in these calculations is to decrease the net annual-mean global radiative forcing by ~20%. Similar fractional reductions of 21% in the net radiative forcing due to the inclusion of clouds were reported by *Berntsen et al.* [1997].

To investigate the effect of ozone perturbations that occur in the stratosphere, ozone perturbations above the assumed tropopause were removed from the calculations. The instantaneous global annual-mean solar and terrestrial radiative forcings were recomputed as +0.09 and +0.30 W m^{-2}, leading to a net radiative forcing of +0.39 W m^{-2}. Thus the radiative effects due to ozone perturbations in the stratosphere caused by increased NO_x emissions in the GCTM of *Levy et al.* [1997] are small. The increase in instantaneous solar radiative forcing and the corresponding decrease in the instantaneous terrestrial radiative forcing is well documented in studies of the radiative effects due to stratospheric ozone depletion [e.g., *Ramaswamy et al.*, 1992]. The effects of stratospheric adjustment on this conclusion are investigated in section 7.

6. Seasonal Cycle

The seasonal cycles of the hemispheric-mean instantaneous net radiative forcings and the column ozone perturbations are shown in Figure 5. Because the radiative forcing is dominated by the terrestrial radiative forcing (see Table 1), the seasonal cycle of the net radiative forcing is a function of the magnitude, spatial distribution, and vertical distribution of the ozone perturbation, and the temperature difference between the surface and the upper troposphere. The seasonal cycle of the radiative forcing in the northern hemisphere is a maximum in July at +0.64 W m^{-2} (+0.51 W m^{-2} terrestrial and +0.13 W m^{-2} solar radiative forcings) and a minimum in January at +0.38 W m^{-2} (+0.31 W m^{-2} terrestrial and +0.07 W m^{-2} solar radiative forcings), while the total ozone perturbation remains in the range 12.7–14.8 DU. The range of the northern hemisphere solar radiative forcing (+0.07 W m^{-2} to +0.13 W m^{-2}) is insufficient to explain the seasonal cycle of the northern hemisphere radiative forcing. While the temperature of the stratosphere and upper troposphere displays little seasonal variation in temperature, the average northern hemispheric surface air temperature varies from 277 K in January to 294 K in July and August. Thus the difference between the surface temperature and the upper troposphere temperature is largest in the summer months, leading to the strongest net radiative forcing. The seasonal cycle in the southern hemisphere shows a maximum radiative forcing in October at +0.36 W m^{-2} (+0.29 W m^{-2} terrestrial and +0.07 W m^{-2} solar radiative forcings) and a minimum in May at +0.19 W m^{-2} (+0.16 W m^{-2} terrestrial and +0.03 W m^{-2} solar radiative forcings). It is interesting to note that the seasonal cycle of the radiative forcing in the southern hemisphere is strikingly similar to the seasonal cycle of the ozone column perturbation; the maximum ozone perturbation is in October when a large amount of biomass burning occurs. The contrast in the behavior of northern hemisphere and southern hemisphere radiative forcing seasonal cycle is due to the zonal-mean southern hemisphere surface air temperature showing much less seasonality in the GCM than in the northern hemisphere because of the higher fractional coverage of oceanic areas. The difference in hemispheric average surface air temperature between January and August is ~7 K for the southern hemisphere but 17 K for the northern hemisphere. Thus in the southern hemisphere the terrestrial radiative forcing tends to be mainly a function of the ozone perturbation rather than of the temperature difference between the surface and the upper troposphere.

7. Adjusted Radiative Forcing

The total sky adjusted radiative forcing is considered to be the most appropriate indicator of climate response [e.g., *IPCC*, 1994, 1996]. To calculate the adjusted radiative forcing, the fixed dynamical heating approximation [e.g., *Fels and Kaplan*, 1975; *Fels et al.*, 1980] is used. However, the stratospheric adjustment process assumes that the timescale of the perturbation causing the radiative forcing is long compared to the timescale for stratospheric adjustment [e.g., *Forster et al.*, 1997]. In the GCM calculations the instantaneous radiative forcing in each grid box will change at each radiation time step (24 hours) due to different cloud distributions, solar cycles, and moisture distributions. It would be possible to perform stratospheric adjustment at each radiation time step. However, in the real atmosphere the stratosphere will not have time to adjust to radiative-dynamical equilibrium because the adjust-

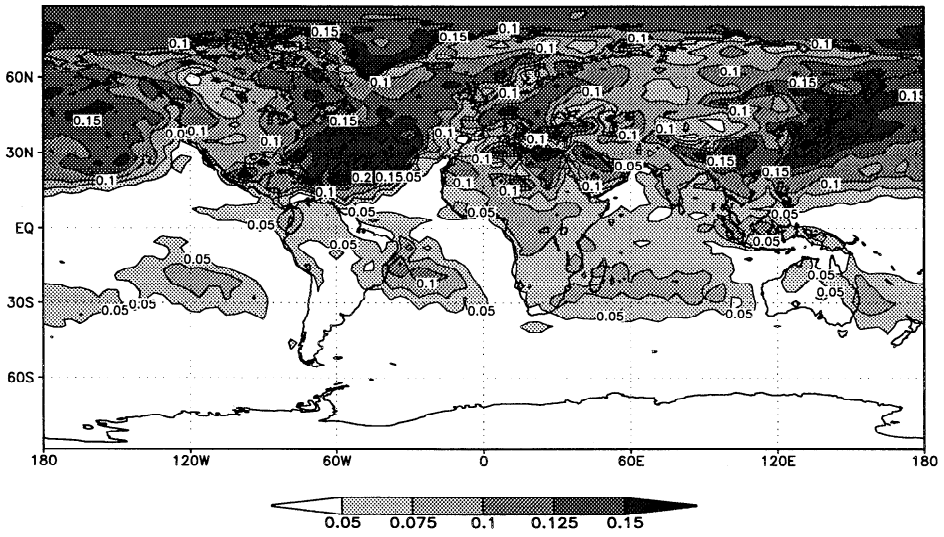

a) NH=+0.10Wm^{-2}, SH=+0.04Wm^{-2}, Global=+0.07Wm^{-2}

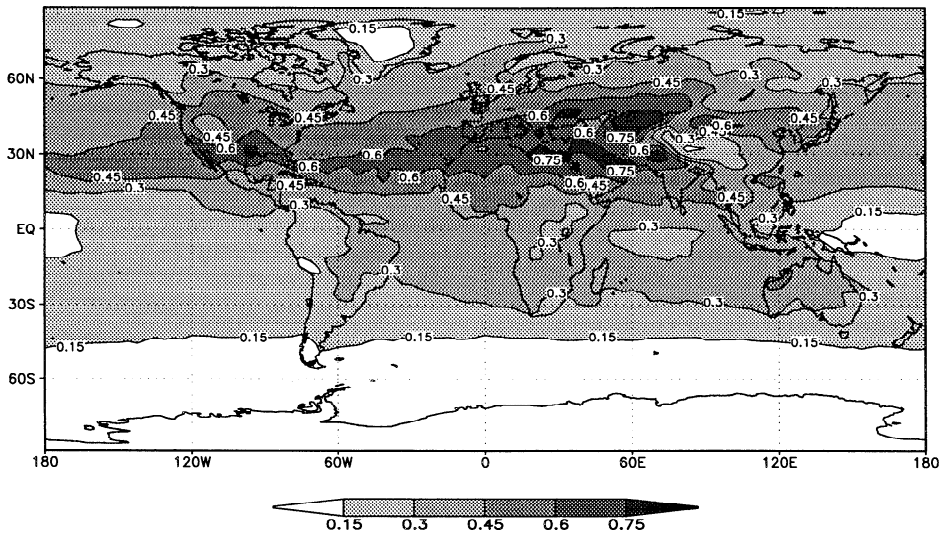

b) NH=+0.41Wm^{-2}, SH=+0.21Wm^{-2}, Global=+0.31Wm^{-2}

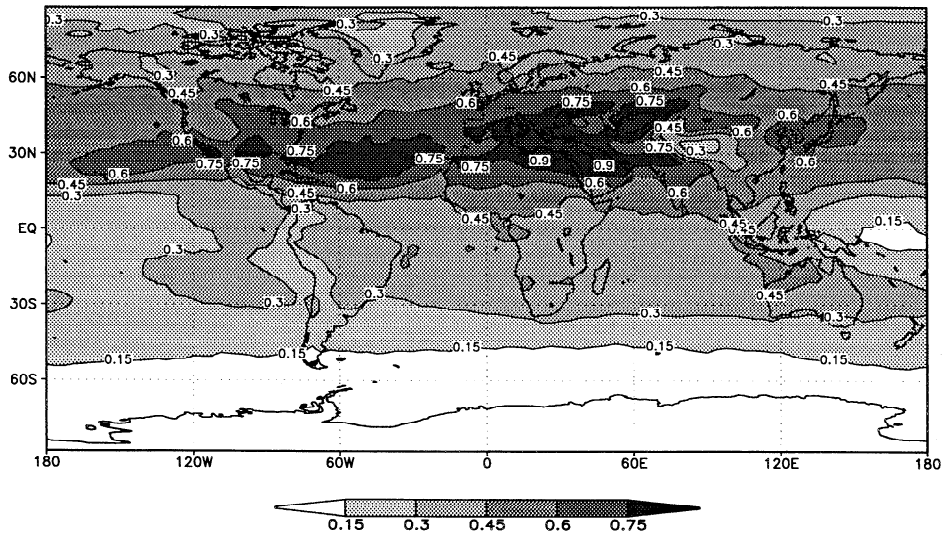

c) NH=+0.51Wm^{-2}, SH=+0.25Wm^{-2}, Global=+0.38Wm^{-2}

Figure 4. (a) Solar, (b) terrestrial, and (c) net instantaneous annual-mean radiative forcing (W m^{-2}), including clouds, using the GCM as described in the text.

ment procedure takes longer than 24 hours. Additionally, calculation of stratospheric adjustment at every radiation time step in the GCM (i.e., every 24 hours) is computationally time consuming. Because the instantaneous radiative forcing from the GCM and the FDHM are similar (see Table 1), the FDHM may be used with monthly mean fields from the GCM to calculate the adjusted radiative forcing (see section 2).

The use of monthly mean input parameters in calculating the radiative forcing in the FDHM causes some small (~10%) differences from the GCM instantaneous radiative forcings (see Table 1). The total annual-mean clear-sky instantaneous radiative forcing at the tropopause in the FDHM is +0.02 W m^{-2} for the solar spectrum and +0.42 W m^{-2} for the terrestrial spectrum, yielding a net clear-sky instantaneous radiative forcing of +0.45 W m^{-2}. Thus the global-mean instantaneous radiative forcing when clouds are excluded is within 3% of that calculated by the GCM (see Figures 3a and 4a). When clouds are included in the calculations, the differences between the FDHM and the GCM global net radiative forcing are larger with the FDHM, giving a radiative forcing some 10% lower than that of the GCM (+0.35 W m^{-2} compared to +0.38 W m^{-2}; see Figure 6a). This may be partly attributable to the fact that the GCM uses an on/off cloud scheme, where a GCM grid box is assumed to be entirely filled with cloud when the relative humidity exceeds a certain threshold, whereas the FDHM uses a fractional cloud amount obtained from the GCM monthly mean cloud fraction diagnostics. Additionally, the cloud overlap and albedos in the FDHM, which are determined from the monthly mean altitude profiles from the GCM, will necessarily be different to the cloud fields calculated at each time step in the GCM.

Despite these differences, the results from the FDHM and the GCM are in reasonable agreement, suggesting that monthly mean variables may be used without introducing significant biases. The adjusted radiative forcing from the FDHM is +0.05 W m^{-2} in the solar spectrum and +0.27 W m^{-2} in the terrestrial spectrum, yielding a net radiative forcing of +0.32 W m^{-2} (Figure 6b). Thus the effect of stratospheric adjustment is to reduce the net instantaneous radiative forcing by ~10%, with all the stratospheric adjustment being due to the terrestrial radiative forcing, which is within the 10–20% range quoted by K. P. Shine and P. M. de F. Forster (The effect of human activity on radiative forcing of climate change, submitted to *Global and Planetary Change*, 1998). The effect of stratospheric adjustment upon the temperature of the stratosphere is to cool the stratosphere by up to 0.5 K zonally, the maximum cooling being located at ~30°N. The adjusted radiative forcing was also calculated excluding any ozone changes in the stratosphere. The annual mean net radiative forcing was found to decrease by a further 10% to +0.29 W m^{-2} due to an increase in the solar radiative forcing from +0.05 to +0.07 W m^{-2} and a corresponding decrease in the terrestrial radiative forcing from +0.27 to +0.22 W m^{-2}.

Table 1. Global Annual-Mean Instantaneous (Inst.) and Adjusted (Adj.) Solar (S.W.), Terrestrial (L.W.), and Net Radiative Forcing at the Tropopause Due to Anthropogenic Tropospheric Ozone Perturbation of *Levy et al.* [1997] Described in Section 3

Case	S.W.	L.W.	Net
Inst. clear (GCM)	+0.02	+0.44	+0.46
Inst. cloudy (GCM)	+0.07	+0.31	+0.38
Adj. cloudy (GCM)*	+0.07	+0.28	+0.35
Adj. cloudy (GCM)*†	+0.09	+0.23	+0.32
Inst. clear (FDHM)	+0.02	+0.42	+0.45
Inst. cloudy (FDHM)	+0.05	+0.29	+0.35
Adj. cloudy (FDHM)	+0.05	+0.27	+0.32
Adj. cloudy (FDHM)†	+0.07	+0.22	+0.29

*The general circulation model (GCM) adjusted radiative forcing is estimated by applying the same fractional adjustment as in the fixed dynamical heating model (FDHM).

†These values correspond to calculations excluding ozone perturbations from the stratosphere.

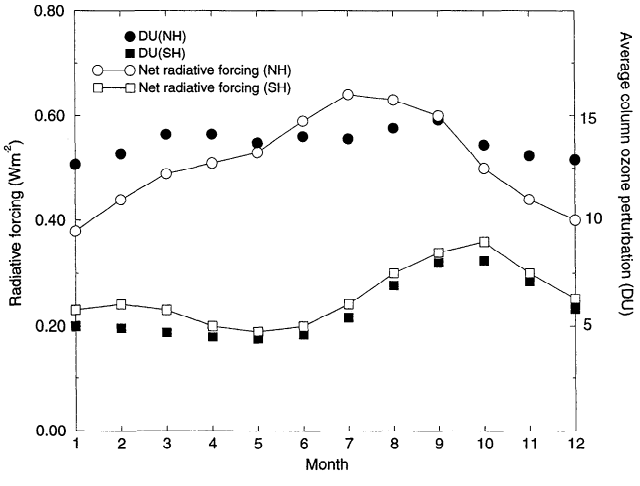

Figure 5. Seasonal cycle of the instantaneous hemispheric radiative forcings (W m^{-2}) and the total column ozone perturbations (DU). Note that total column burdens are shown here. The contribution from the troposphere is approximately 78% ± 4% throughout the seasonal cycle. The adjusted radiative forcing is ~10% lower than the instantaneous radiative forcing throughout the seasonal cycle.

8. Discussion and Conclusions

The adjusted radiative forcing due to modeled ozone perturbations is estimated by the FDHM to be +0.05 W m^{-2} in the solar spectrum and +0.27 W m^{-2} in the terrestrial spectrum, yielding a total net adjusted radiative forcing of +0.32 W m^{-2} which is approximately 10% lower than the instantaneous radiative forcing. If the ozone perturbations in the stratosphere from the GCTM of *Levy et al.* [1997] are removed from the calculations, the net radiative forcing is reduced by a further 10%. This estimate of the adjusted radiative forcing has an associated uncertainty of ~10% due solely to the use of monthly mean fields (particularly cloud fields) rather than daily data as input to the radiation code.

The spatial pattern of the adjusted radiative forcing is substantially different from present-day estimates of the radiative forcing due to anthropogenic emissions of well-mixed greenhouse gases (e.g., carbon dioxide) which exert a radiative forcing in the terrestrial spectrum ranging from approximately +1.5 W m^{-2} at the poles to approximately +3.0 W m^{-2} at the equator [e.g., *Kiehl and Briegleb*, 1993]. The approximate hemispheric symmetry that is seen for well-mixed greenhouse gases is not seen for perturbations in tropospheric ozone. For tropospheric ozone perturbations the northern hemisphere annual-mean radiative forcing is approximately double that of the southern hemisphere. The spatial pattern of the radiative forc-

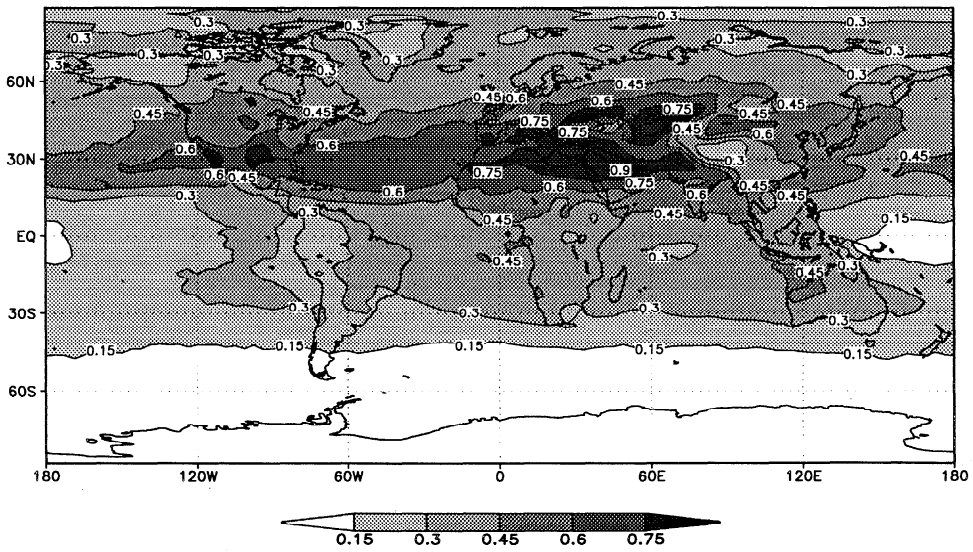

a) NH=+0.46Wm^{-2}, SH=+0.23Wm^{-2}, Global=+0.35Wm^{-2}

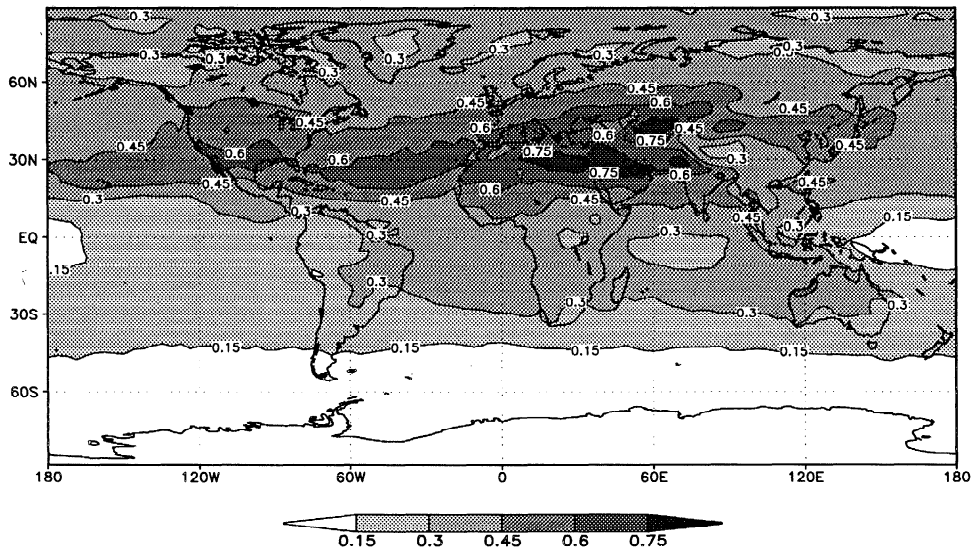

b) NH=+0.43Wm^{-2}, SH=+0.21Wm^{-2}, Global=+0.32Wm^{-2}

Figure 6. (a) Instantaneous and (b) adjusted annual-mean radiative forcing (W m^{-2}) using the fixed dynamical heating model as described in the text.

ing is also different to the radiative forcing exerted by tropospheric sulfate and black carbon [*Haywood et al.*, 1997a; *Haywood and Ramaswamy*, 1998]. Additionally, unlike sulfate and black carbon aerosols, 85% of the radiative forcing in our calculations occurs in the terrestrial spectrum. The spatial pattern also differs markedly from the pattern of direct radiative forcing due to mineral dust which may be positive or negative depending on the spatial and size distribution of the particles, the surface reflectance, and the cloud amount [*Tegen et al.*, 1996]. *Shine and Forster* [1998] show the spatial pattern of estimates of the radiative forcing of all of these different species in their recent review.

Sections 3 and 7 showed that a tropospheric perturbation of 86 Tg (7.9 DU) leads to an estimated adjusted radiative forcing of between +0.29 W m^{-2} and +0.32 W m^{-2}. Thus the sensitivity of the radiative forcing to tropospheric ozone column perturbation in these calculations is estimated as approximately +0.038 W m^{-2}/DU. The adjusted radiative forcing is in excellent agreement with the +0.28 W m^{-2} to +0.31 W m^{-2} estimated by *Berntsen et al.* [1997] and the +0.30 W m^{-2} estimated by *Forster et al.* [1996], as are the results from the clear-sky and instantaneous forcing calculations. However, the tropospheric perturbation used in these two studies is 102 Tg (9.4 DU), suggestive of a somewhat lower sensitivity of +0.032 W m^{-2}/DU. Additionally, some studies suggest a rather higher sensitivity to that found here; the recent 3-D modeling study of *Roelofs et al.* [1997] reports an adjusted radiative forcing of +0.42 W m^{-2} for a tropospheric ozone perturbation of ~7.3 DU and thus a sensitivity of approximately +0.058 W m^{-2}/DU. Reasons for the different sensitivities include the use of different geographic and vertical distributions of the ozone perturbations, different atmospheric profiles of temperature and humidity, different cloud and surface reflectance fields, and different radiative transfer codes. Determining which of

the chemical transport models best represents the anthropogenic ozone perturbation is a difficult task because both the past and the present ozone concentrations must be modeled accurately. The paucity of historical observations of ozone at the surface and at higher altitudes present significant problems in determining the spatial distribution of the anthropogenic perturbation. Additionally, present-day measurements of ozone in the upper troposphere are only available from a limited number of sondes at specific sites. Furthermore, it is difficult to ascertain how much of the observed perturbations in the upper troposphere is due to tropospheric chemistry and how much is due to anomaly propogation from the stratosphere.

These results suggest that the radiative forcing due to changes in tropospheric ozone are of a comparable magnitude to the direct radiative forcing due to sulfate aerosol (e.g., -0.28 W m^{-2} from *Kiehl and Briegleb* [1993], -0.29 W m^{-2} from *Boucher and Anderson* [1995], and -0.38 W m^{-2} from *Haywood et al.* [1997a]). Thus coupled ocean-atmosphere studies that include only the effects of well-mixed greenhouse gases and sulfate aerosols [e.g., *Mitchell et al.*, 1995; *Haywood et al.*, 1997b; *Meehl et al.*, 1996] should be further extended to include other gaseous and aerosol species of anthropogenic origin.

Acknowledgments. Thanks are due to Chip Levy and Prasad Kasibhatla for providing the ozone climatologies. Piers Forster and another anonymous referee are thanked for their useful comments on an earlier version of the manuscript.

References

Berntsen, T., I. S. A. Isaksen, G. Myhre, J. S. Fuglestvedt, F. Stordal, T. Alsvik Larsen, R. S. Freckleton, and K. P. Shine, Effects of anthropogenic emissions on tropospheric ozone and its radiative forcing, *J. Geophys. Res.*, *102*, 28,101–28,126, 1997.

Boucher, O., and T. L. Anderson, GCM Assessment of the sensitivity of direct climate forcing by anthropogenic sulfate aerosols to aerosol size and chemistry, *J. Geophys. Res.*, *100*, 26,117–26,134, 1995.

Chalita, S., D. A. Hauglustaine, H. Le Treut, and J.-F. Muller, Radiative forcing due to increased tropospheric ozone concentrations, *Atmos Environ.*, *30*, 1641–1646, 1994.

Cooke, W. F., and J. J. N. Wilson, A global black carbon model, *J. Geophys. Res.*, *101*, 19,395–19,409, 1996.

Fels, S. B., and L. D. Kaplan, A test of the role of longwave radiative transfer in a general circulation model, *J. Atmos. Sci.*, *33*, 779–789, 1975.

Fels, S. B., J. D. Mahlman, M. D. Schwarzkopf, and R. W. Sinclair, Stratospheric sensitivity to perturbations in ozone and carbon dioxide: Radiative and dynamical response, *J. Atmos. Sci.*, *37*, 2265–2297, 1980.

Forster, P. M. de F., C. E. Johnson, K. S. Law, J. A. Pyle, and K. P. Shine, Further estimates of radiative forcing due to tropospheric ozone changes, *Geophys. Res. Lett.*, *23*, 3321–3324, 1996.

Forster, P. M. de F., R. S. Freckleton, and K. P. Shine, On aspects of the concept of radiative forcing, *Clim. Dyn.*, *13*, 547–560, 1997.

Freidenreich, S. M., and V. Ramaswamy, A new multi-band solar radiative parameterization, in *Ninth Conference on Atmospheric Radiation*, pp. 129–130, Am. Meteorol. Soc., Boston, Mass., 1997.

Hauglustaine, D. A., C. Granier, G. P. Brasseur, and G. Megie, The importance of atmospheric chemistry in the calculation of radiative forcing on the climate system, *J. Geophys. Res.*, *99*, 1173–1186, 1994.

Haywood, J. M., and V. Ramaswamy, Global sensitivity studies of the direct radiative forcing due to anthropogenic sulfate and black carbon aerosol, *J. Geophys. Res.*, *103*, 6043–6058, 1998.

Haywood, J. M., D. L. Roberts, A. Slingo, J. M. Edwards, and K. P. Shine, General circulation model calculations of the direct radiative forcing by anthropogenic sulphate and fossil-fuel soot aerosol, *J. Clim.*, *10*, 1562–1577, 1997a.

Haywood, J. M., R. J. Stouffer, R. Wetherald, S. Manabe, and V. Ramaswamy, Transient response of a coupled model to estimated changes in greenhouse gas and sulfate concentrations, *Geophys. Res. Lett.*, *24*, 1335–1338, 1997b.

Intergovernmental Panel on Climate Change (IPCC), *Climate Change: The Scientific Assessment*, edited by J. T. Houghton, G. J. Jenkins, and J. J. Ephraums, Cambridge Univ. Press, New York, 1990.

IPCC, *Climate Change 1994: Radiative Forcing of Climate Change and An Evaluation of the IPCC IS92 Emission Scenarios*, edited by J. T. Houghton, L. G. Meira Filho, J. Bruce, H. Lee, B. A. Callander, E. Haites, N. Harris, and K. Maskell, Cambridge Univ. Press, New York, 1994.

IPCC, *Climate Change 1995: The Science of Climate Change*, edited by J. T. Houghton, L. G. Meira Filho, B. A. Callander, N. Harris, A. Kattenberg, and K. Maskell, Cambridge Univ. Press, New York, 1996.

Kasibhatla, P., W. L. Chameides, and J. St. John, A three-dimensional global model investigation of the seasonal variation in the atmospheric burden of anthropogenic sulfate aerosols, *J. Geophys. Res.*, *102*, 3737–3759, 1997.

Kiehl, J. T., and B. P. Briegleb, The relative roles of sulfate aerosols and greenhouse gases in climate forcing, *Science*, *260*, 311–314, 1993.

Lacis, A. A., and J. E. Hansen, A parameterization for the absorption of solar radiation in the Earth's atmosphere, *J. Atmos. Sci.*, *31*, 118–131, 1974.

Lacis, A. A., D. J. Wuebbles, and J. A. Logan, Radiative forcing of climate by changes in the vertical distribution of ozone, *J. Geophys. Res.*, *95*, 9971–9981, 1990.

Levy, H., II, P. S. Kasibhatla, W. J. Moxim, A. A. Klonecki, J. I. Hirsh, S. J. Oltmans, and W. L. Chameides, The global impact of human activity on tropospheric ozone, *Geophys. Res. Lett.*, *24*, 791–794, 1997.

Liousse, C., J. E. Penner, C. Chuang, J. J. Walton, and H. Eddleman, A global three-dimensional model study of carbonaceous aerosols, *J. Geophys. Res.*, *101*, 19,411–19,432, 1996.

Marenco, A., H. Gouget, P. Nedelec, J.-P. Pages, and F. Karcher, Evidence of long-term increase in tropospheric ozone from Pic du Midi data series: Consequences: Positive radiative forcing, *J. Geophys. Res.*, *99*, 16,617–16,632, 1994.

Meehl, G. A., W. M. Washington, D. J. Erickson III, B. P. Briegleb, and P. J. Jaumann, Climate change from increased CO_2 and direct and indirect effects of sulfate aerosols, *Geophys. Res. Lett.*, *23*, 3755–3758, 1996.

Mitchell, J. F. B., T. C. Johns, J. M. Gregory, and S. F. B. Tett, Climate response to increasing levels of greenhouse gases and sulphate aerosols, *Nature*, *376*, 501–504, 1995.

Ramaswamy, V., D. M. Schwarzkopf, and K. P. Shine, Radiative forcing of climate from halocarbon-induced global stratospheric ozone loss, *Nature*, *355*, 810–812, 1992.

Roelofs, G.-J., J. Lelieveld, and R. van Dorland, A three-dimensional chemistry/general circulation model simulation of anthropogenically derived ozone in the troposphere and its radiative climate forcing, *J. Geophys. Res.*, *102*, 23,389–23,401, 1997.

Schwarzkopf, D. M., and S. B. Fels, The simplified exchange method revisited: An accurate, rapid method for computation of infrared cooling rates and fluxes, *J. Geophys. Res.*, *96*, 9075–9096, 1991.

Tegen, I., and I. Fung, Contribution to the atmospheric mineral aerosol load from land surface modification, *J. Geophys. Res.*, *100*, 18,707–18,726, 1995.

Tegen, I., A. A. Lacis, and I. Fung, The influence of mineral aerosols from disturbed soils on climate forcing, *Nature*, *380*, 419–422, 1996.

Wetherald, R., and B. Soden, General simulation of atmospheric temperature and moisture in the GFDL AMIP experiment, in *Proceedings of the First International AMIP Scientific Conference*, *WCRP-92*, *WMO/TD-732*, pp. 97–100, World Meteorol. Organ., Geneva, 1995.

World Meteorological Organization (WMO), Scientific assessment of stratospheric ozone depletion: 1994 Global ozone research and monitoring project, *WMO Rep. 37*, Geneva, 1995.

J. M. Haywood, Meteorological Research Flight, Y46 Bldg., DERA, Farnborough, Hants, GU14 0LX, UK. (e-mail: jmhaywood@meto.gov.uk)

M. D. Schwarzkopf and V. Ramaswamy, Geophysical Fluid Dynamics Laboratory (GFDL), Princeton University, Princeton, NJ, 08542.

(Received November 11, 1997; revised March 26, 1998; accepted April 14, 1998.)